THE SCIENTIFIC TEMPER (2026) Vol. 17 (3): 5736-5745

E-ISSN: 2231-6396, ISSN: 0976-8653

Doi: 10.58414/SCIENTIFICTEMPER.2026.17.3.01

https://scientifictemper.com/

RESEARCH ARTICLE

Density Functional Theory calculations, Spectroscopic study, Reduced Density Gradient and molecular docking of 2-[3-(4-chlorophenyl)-5-(4-(propane-2-yl) phenyl-4, 5-dihydro-1H pyrozol-1-yl]-4-(nitrophenyl)-1, 3-thiazole

S. Babiyana[1], V. Balachandran[2*]

Abstract

The 2-[3-(4-chlorophenyl)-5-(4-(propane-2-yl) phenyl-4,5-dihydro-1Hpyrozol-1-yl]-4-(nitrophenyl)-1,3-thiazole (CPDNT) was synthesized by reflux technique. FT-IR and FT-Ramanstudies attest to the presence of functional groups in the 2CPDNT molecule together with DFT method. Vibrational assignments were done using scaled quantum mechanical force fields. To assess the molecule's chemical reactivity, the highest occupied molecular orbital (HOMO) and the lowest unoccupied molecular orbital (LUMO) energy gap and quantum chemical descriptors were computed using the frontier orbital energies. A Molecular Electrostatic Potential (MEP) Map is a powerful means for visualizing the electron density distribution of a molecule, helping to identify its electrophilic and nucleophilic regions. Theoretical topology analysis (ELF, LOL) has been performed. A Reduced Density Gradient (RDG) was applied to examine weak interactions. To find the protein-ligand interaction and its lowest binding energy, the CPDNT molecule was docked to the active sites of 1FSE, 3VZX, 5MKD, and LIXM protein structures.

Keywords: DFT; Thiazole; RDG; ELF; MEP; Docking.

Introduction

The synthesis of heterocyclic compounds is seen as beneficial in the field of drug discovery. Individuals possessing penta-cyclic structures exerted a significant influence on heterocyclic molecules within the domains of chemistry and biology (Roy et al., 2024). Thiazole nuclei exhibit a diverse range of biological functions, which is a noteworthy observation. The presence of a five-member ring distinguishes thiazole. Thiazole derivatives have attracted the attention of scientists due to their diverse pharmacological effects (Patra et al., 2021). Thiazole compounds exhibit potential as anticancer, antibacterial, and antiviral drugs (Cashman et al., 2020, Moeini et al., 2019, Kassem et al., 2024, Liu et al., 2024). Synthetic drugs with a thiazole core include antibiotics like sulfathiazole and penicillin, cancer drugs like bleomycin and tiazofurin, HIV drugs, and ulcer treatments. Additionally, extensively applied thiazole derivatives (Matta et al., 2023, Shosha et al., 2025, Bhanwala et al., 2023, Chahal et al., 2023, Ghomashi et al., 2023) include the non-steroidal drug. The thiazole derivatives significantly influence the pharmacocores of numerous pharmaceutically significant bio compounds. It is desirable to estimate their biotic action, such as antibacterial, anti-tubercular, and anti-fungal properties, especially for their anti-inflammatory properties (Bhasker et al., 2024, Safaei et al., 2012, Saranya et al., 2024, Bachhar et al., 2024,

[1]Department of Physics, Holy Cross College (Autonomous), (Affiliated to Bharathidasan University), Tiruchirappalli 620 002, Tamil Nadu, India

[2]Department of Physics, Arignar Anna Government Arts College (Affiliated to Bharathidasan University), Musiri, Tiruchirappalli 621 211, Tamil Nadu, India

***Corresponding Author:** V. Balachandran, Department of Physics, Arignar Anna Government Arts College (Affiliated to Bharathidasan University), Musiri, Tiruchirappalli 621 211, Tamil Nadu, India, E-Mail: brsbala66@gmail.com

How to cite this article: Babiyana, S., Balachandran, V. (2026). Density Functional Theory calculations, Spectroscopic study, Reduced Density Gradient and molecular docking of 2-[3-(4-chlorophenyl)-5-(4-(propane-2-yl) phenyl-4, 5-dihydro-1H pyrozol-1-yl]-4-(nitrophenyl)-1, 3-thiazole. The Scientific Temper, **17**(3):5736-5745.

Doi: 10.58414/SCIENTIFICTEMPER.2026.17.3.01

Source of support: Nil

Conflict of interest: None.

Received: 01/02/2026 **Accepted:** 05/02/2026 **Published :** 25/03/2026

Nemeikaitė-Čėnienė et al., 2023, Sebutsoe et al., 2024, Zheng et al., 2023, Raveesha et al., 2022)

Research on pyrazoline derivatives is extensive due to their presence in numerous pharmacologically active drugs. Pyazofurin, sulfinpyrazone, and metamizole are examples of pharmacological actions associated with pyrazoline function. Furthermore, studies have demonstrated the antioxidant, antibacterial, analgesic, anti-inflammatory, anticonvulsant, antitubercular, antiviral, and anticancer properties of these compounds.

For the title compound, we investigate the structure of the molecules and how charges move within the CPDNT molecules using spectral and quantum chemical calculations. Combining experimental data with theoretical structure analysis utilizing DFT quantum chemical computation gave this result. We used density functional theory to calculate vibrational and optimized geometry at the B3LYP/cc-pVDZ levels. We also performed frontier molecular orbital analysis and molecular electrostatic potential calculations. We used molecular docking to find the possible modes for the CPDNT molecule to bind to protein-active sites in Bacillus subtilis.

Materials and Methods

2-[3-(4-chlorophenyl)-5-(4-(propane-2-yl)phenyl-4,5-dihydro-1Hpyrozol-1-yl]-4-(nitrophenyl)-1,3-thiazole was synthesized by refluxing 3-(4-chlorophenyl)-5-[4-propan-2-yl) phenyl]-4,5-dihydro-1H-pyrazole-1-carbothioamide (0.01mol) and 2-(bromomethyl)-4-methoxyphenol (0.01mol in ethanol/DMF mixture (30ml) as per the procedure reported. (Babiyana et al., 2024).

Characterization details

The FT-IR spectrum of the compound was recorded employing a Perkin Elmer spectrometer fitted with a KBr beam splitter around 4000 –450 cm^{-1}. Bruker RFS 27 FT-Raman spectrometer was used to report the FT-Raman spectrum in the region 3500 – 0 cm^{-1} using a 1064 nm Nd: YAG laser source.

Quantum chemical calculations

We used the DFT/B3LYP/cc-pVDZ basis sets to calculate the structural properties of the CPDNT molecule. We performed the calculations using the Gaussian 09W program (Frisch et al., 2009, Parr et al.,1995, Dennington et al., 2009). We used an isolated CPDNT molecule's optimized molecular structure to calculate vibrational and other quantum chemical calculations. The Gauss View 5.0 graphical interface (Viji et al., 2020) visualized the frontier molecular orbital and MEP surfaces of CPDNT. The Multiwfn software maps the CPDNT molecule's reduced gradient densities and represents them through the VMD program. This lets us insight at the topology of the non-covalent interaction in line with Bader's theory.

Results and Discussion

Optimized geometry

Figure 1 displays the optimized molecular structure of the CPDNT molecule. The theoretical geometrical parameters of CPDNT are depicted in Table1 using B3LYP/cc pVDZ. C-C bond length is in the range of 1.410–1.378 Å (Şahin et al., 2024). C-C bond lengths of C1-C2 and C2-C3 are 1.399Å and 1.391Å and this calculated value shows an excellent agreement with the experimental value.

C-N bond length 1.351/1.381Å is greater than C=N (1.22 Å). In the present study, the C-N bond lengths of C12-N14 and C51-N54 are 1.324 Å and 1.485 Å, which is in good accordance with the observed value. C-H bond lengths of C3-H8, C13-H58, C21-H23and C26-H30are 1.101, 1.116, 1.089 and 1.101 Å which matches with experimental value (Ragavan, et al., 2022).

Vibrational study

The CPDNT molecule used in this investigation has 58 atoms and 168 normal vibrational modes are computed at the B3LYP/cc-pVDZ levels. Table 2 presents the vibrational assignments of CPDNT with PED contributions. Using the VEDA 4 algorithm (Vidya et al., 2019), Potential Energy Distribution (PED) assigns expected infrared and Raman vibrational wavenumbers. Fig.2. and Fig.3. shows computed and investigational FT-IR and FT-Raman spectra.

CH vibration

The range of symmetric vibrations is 2990-2900 cm^{-1}, while the range of asymmetric (C-H stretching) vibrations is 3100-3000 cm^{-1} (Neetha et al., 2025). The bands for the main compound were found at 3174, 3116, 2922 cm^{-1}(FT-IR) and 3077, 2932 cm^{-1}(FT-Raman). The DFT estimated value is 3176 and 3118$cm^{-1}$with a 99% (PED) contribution. Bands in the 1300-1000 cm^{-1} area are typically used to describe the strong to weak intensity of the C-H bending vibrations (Elangovan et al., 2024). Around 1283-909 cm^{-1} (in-plane)

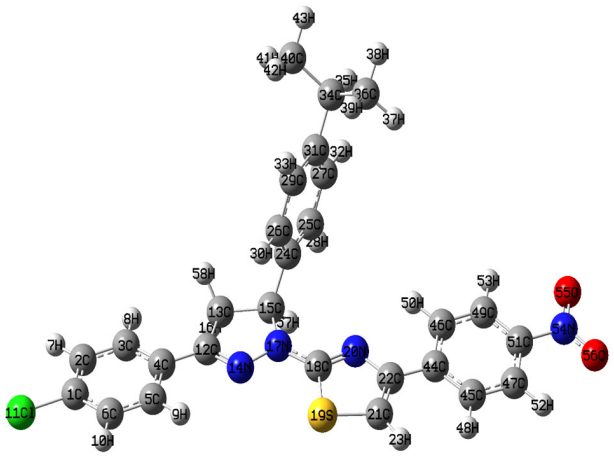

Figure 1: Optimized structure of CPDNT molecule

Table 1: Optimized geometrical parameters of CPDNT compound

Bond lengths	*B3LYP*	*Bond*	*B3LYP*	*Dihedral*	*B3LYP*
	(Å)	*angles*	*(Å)*	*Angles*	*(Å)*
C1-C2	1.399	C2-C1-C6	120.36	C6-C1-C2-C3	-0.01
C1-C6	1.398	C2-C1-Cl11	119.76	C6-C1-C2-H7	-179.98
C1-Cl11	1.698	C6-C1-Cl11	119.88	Cl11-C1-C2-C3	179.98
C2-C3	1.391	C1-C2-C3	119.65	Cl11-C1-C2-H7	0.00
C2-H7	1.101	C1-C2-H7	120.34	C2-C1-C6-C5	-0.04
C3-C4	1.404	C3-C2-H7	120.01	C2-C1-C6-H10	179.96
C3-H8	1.101	C2-C3-C4	120.59	Cl11-C1-C6-C5	179.98
C4-C5	1.403	C2-C3-H8	119.23	Cl11-C1-C6-H10	-0.02
C4-C12	1.456	C4-C3-H8	120.18	C1-C2-C3-C4	0.08
C5-C6	1.393	C3-C4-C5	119.18	C1-C2-C3-H8	-179.92
C5-H9	1.102	C3-C4-C12	119.64	H7-C2-C3-C4	-179.94
C6-H10	1.101	C5-C4-C12	121.18	H7-C2-C3-H8	0.06
C12-C13	1.523	C4-C5-C6	120.47	C2-C3-C4-C5	-0.11
C12-N14	1.324	C4-C5-H9	120.40	C2-C3-C4-C12	179.72
C13-C15	1.557	C6-C5-H9	119.14	H8-C3-C4-C5	179.89
C13-H16	1.115	C1-C6-C5	119.74	H8-C3-C4-C12	-0.28
C13-H58	1.116	C1-C6-H10	120.36	C3-C4-C5-C6	0.07
N14-N17	1.368	C5-C6-H10	119.90	C3-C4-C5-H9	-179.90
C15-N17	1.512	C4-C12-C13	121.60	C12-C4-C5-C6	-179.76
C15-C24	1.497	C4-C12-N14	125.48	C12-C4-C5-H9	0.27
C15-H57	1.128	C13-C12-N14	112.90	C3-C4-C12-C13	3.82
N17-C18	1.416	C12-C13-C15	101.67	C3-C4-C12-N14	-177.75
C18-S19	1.741	C12-C13-H16	111.41	C5-C4-C12-C13	-176.36
C18-N20	1.348	C12-C13-H58	111.10	C5-C4-C12-N14	2.08
S19-C21	1.658	C15-C13-H16	111.50	C4-C5-C6-C1	0.01
N20-C22	1.393	C15-C13-H58	111.44	C4-C5-C6-H10	-179.99
C21-C22	1.396	H16-C13-H58	109.54	H9-C5-C6-C1	179.98

and 832-710 cm–1 (out-of-plane), the C-H bending vibrations were observed. The present compound had C-H bending at 1176 cmcm^{-1}(FT-Raman) and DFT values were the same at 1178cm^{-1}(70% PED). With corresponding DFT values at 1164 cm^{-1} (72% PED), C-H (in-plane) bending was detected at 1165 cm^{-1} (FT-IR). There is a noticeable bending vibration in the 1000–750 cm^{-1} (out-of-plane) region. The bending (out-of-plane) vibration in the current study was measured at 853 cm^{-1} (FT-IR) and 852 cm^{-1} (FT-Raman), with an estimated value of 852 cm^{-1} (69% PED).

CH_2 vibrations

The range of CH_2 antisymmetric stretching vibrations is 3100-3000 cm^{-1}, while the range of symmetric stretching is 3000-2900 cm^{-1} (Elangovan et al., 2024). In FT-IR, symmetric CH_2 vibrations are seen at 2857 cm^{-1}, which agrees with the calculated asymmetric CH_2 vibrations seen at 2861 cm^{-1}(99% PED). The CH_2 twisting vibrations are at 1128 cm^{-1}in FT-IRand DFT is calculated to be 1130 cm^{-1}(61% PED). The peak at 1407 cm^{-1} (FT-IR) and peak at 1403 cm^{-1}(FT-Raman) are both attributed to CH_2 scissoring, with the estimated value at 1408 cm^{-1} (69% PED).

CH_3 vibrations

The CH_3 (symmetric) stretching mode is estimated to be around 2870 cm^{-1}, whereas the asymmetric CH_3 stretching is at 2980 cm^{-1}. CH_3 stretching (asymmetric) has a magnitude greater than the CH_3 stretching (symmetric). CH_3 stretching vibrations are anticipated in the range of 3050–2800 cm^{-1}(Vidya et al., 2019, Neetha et al., 2025). The bands at

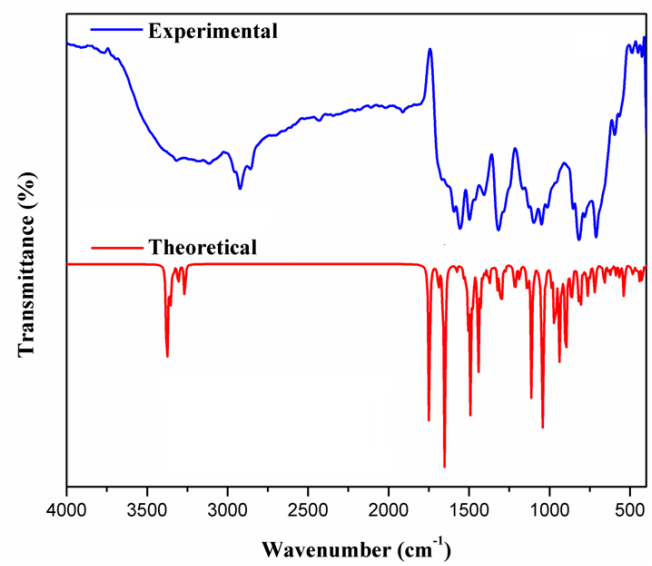

Figure 2: Experimental and theoretical FT-IR spectra of CPDNT compound

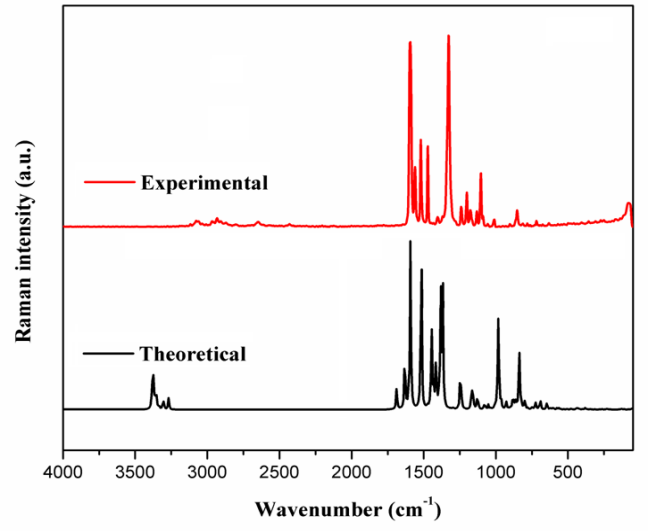

Figure 3: Experimental and theoretical FT-Raman spectra of CPDNT compound

2922 cm^{-1} in FT-IR and 2932 cm^{-1} in FT-Raman are assigned to CH_3 asymmetric stretching. The corresponding DFT value is observed at 2928$cm^{-1}$and 2936 $cm^{-1}$with 98 % PED. Deformation is detected in the range 1450-1400 cm^{-1}(Vidya et al., 2019). The experimental peaks detected at 1317 cm^{-1}(FT-IR) match the calculated bending deformations presented at 1318 cm^{-1} with a 78% PED contribution. Peaks were detected at 1012 cm^{-1}(FT-IR) and 1011 cm^{-1}(FT-Raman), while the estimated bending (in -plane) deformations in DFT were found at 1015 cm^{-1} with 71% PED contribution.

C-C and C-N vibrations

C-C stretching vibrations occur in between 1380-1280 cm^{-1}, and C=C stretching vibrations occur in between 1625-1400 cm^{-1}(Vidya et al., 2019). In the current study, the peaks were detected at 1593 cm^{-1}(FT-IR) and 1594 cm^{-1} (FT-Raman). DFT value is observed at 1604 $cm^{-1}$with 96% PED. The peak was detected at 1555 cm^{-1}(FT-IR) with DFT values at 1563 cm^{-1}(68%). The C-N stretching vibration occurs between 1382-1266 cm^{-1} and 1310-1290 cm^{-1}. C-N stretching absorption is assigned at 1348 cm^{-1} (80% PED) for the title compound.

NO_2 vibrations

NO_2 bending (symmetric) occurs in the range 1370 - 1330 cm^{-1}. Symmetrical NO_2 vibrations occur at 1326 cm^{-1} in FT-Raman, which matches with the computed (symmetric) vibrations observed at 1328 cm^{-1} with 86% PED.

Ring vibrations

Experimental values at 566 $cm^{-1}$and 568 $cm^{-1}$for FT-IR and FT-Raman were attributed to ring vibrations (in-plane bending) and the corresponding observed values at 570 $cm^{-1}$with 72% PED. Ring vibrations at 450 cm^{-1}in the FT-IR and the estimated value at 452 cm^{-1}(70% PED).

Frontier molecular orbital analysis

There is a relationship between the property of frontier molecular orbitals with the optical, electrical, and UV-vis spectra of a molecule. The three-dimension plot of the highest HOMO and LUMO of CPDNT are shown in Fig. 4. The energy gap (eV) was a very important dispute to analyze the chemical behavior of the title compound (Şahin et al.,2024). In Fig.4. HOMOs are concentrated on the Cl11 atom, C2-C1-C6, C3-C4-C5, C13-C12-N14, C13-H58, C13-H16, C15-N17, C15-C24, C15-H57, C18-N20, S19 atom, C21-C22, C45, C46 atoms and C51-N54. As well as LUMOs are localized on the N54, O55 and O56 atoms of the nitro group, C51 atom, C45-C47, C44, C21, C22, S19, C18, N20 and C46-C49. The calculated values of HOMO and LUMO, as well as its respective energy gap, have been calculated to be -5.555 eV, -2.344 eV, and 3.211

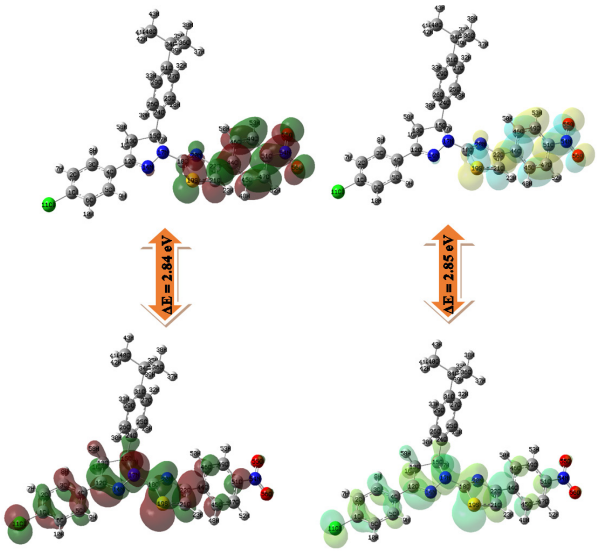

Figure 4: HOMO-LUMO of CPDNT

Table 2: Vibrational assignments, observed and calculated wavenumbers of CPDNT compound

Observed wavenumbers (cm^{-1})		*Calculated wavenumbers (cm^{-1})*	*Vibrational assignments*
FT-IR	*FT-Raman*	*B3LYP/6311++G(d,p)*	*(%PED)*
3174	-	3176	ν CH(99)
3116	-	3118	ν CH(99)
-	-	3112	ν CH(99)
-	-	3091	ν CH(99)
-	3077	3082	ν CH(98)
-	-	3051	ν CH(98)
-	-	3039	ν CH(98)
-	-	3017	ν CH(99)
-	-	2989	ν CH(98)
-	-	2973	ν CH(99)
-	-	2948	ν CH(98)
-	2932	2936	ν CH(98)
2922	-	2928	ν CH(98)
-	-	2918	ν_{ass} CH_3(98)
-	-	2910	ν_{ass} CH_3(98)
-	-	2901	ν_{ass} CH_3(98)
-	-	2887	ν_{ass} CH_2(98)
-	-	2880	ν_{ass} CH_3(98)
-	-	2874	ν CH(99)
2857	-	2861	ν_{ass} CH_2(99)
-	-	2848	ν_{ass} CH_3(99)
-	-	2839	ν_{ass} CH_3(99)
-	-	2833	ν CH(98)
1593	1594	1604	ν CC(96),δCH(23)
-	-	1586	$\nu_{ass}NO_2$(63), ν CC(16), δCN(15)
-	-	1577	ν CN(72), ν CC(14), δCH(12)
	1560	1566	ν CC(74), δCH(13)
1555	-	1563	ν CC(68), δCH(15), ν CN(10)
	-	1533	ν CC(68), δCH(18)
-	1520	1523	$\nu_{ass}NO_2$(65), ν CN(16), ν CC(10)
-	-	1516	ν CC(66), $\nu_{ass}NO_2$(23)
-	-	1512	ν CC(65), δCH(21)
-	-	1509	ν CC(72), δCH(12)
1497	-	1498	δCH(69), ν CC(13)
-	-	1475	δCH(81)
-	1472	1454	δCH(80)
-	-	1446	δ_{opb} CH_3(84)
-	-	1433	δ_{opb} CH_3(84)
-	-	1420	δ_{ipb} CH_3(82)
1407	1403	1408	$\sigma_{scirs}CH_2$(69)
-	-	1398	δ_{ipb} CH_3(80)
-	-	1387	δCH(73)
-	-	1380	δCH(75)
-	-	1354	δCH(75)
-	-	1348	ν CN(80), δCH(22)
-	-	1334	δ_{SS} CH_3(78)
-	1326	1328	$\nu_{ss}NO_2$(86)
1317	-	1318	δ_{SS} CH_3(78)
-	-	1311	δCH(78)
-	-	1298	ν CC(69), δCH(12)
-	-	1290	δCH(75), δCC(17)
-	-	1280	ν CC(76), δCH(13)
-	-	1268	δCH(75), δCC(13)
-	-	1254	δCH(86)
-	1240	1246	δCH(68), ν CC(17)
-	-	1235	δCH(68), ν CC(12)
-	-	1228	δCH(68)
-	-	1219	δCH(68)
-	-	1213	δCH(71)
-	1202	1204	δCH(71)
-	-	1196	ρ_{rock} CH_2(68)
-	-	1188	δCH(72)
-	-	1185	δCH(72)
-	1176	1178	δCH(70)
1165	-	1164	δCH(72)
	-	1138	δCH(71)
	1132	1134	δCH(72)
1128	-	1130	τ CH_2(61), γCH(19)
	-	1116	$\gamma_{opr}CH_3$(63)
-	1104	1110	ν NN(76)
1098	-	1096	δ CH(66),νCC(10)
-	1089	1090	δ CH(66)
-	-	1076	νCN(63)
-	-	1065	$\gamma_{opr}CH_3$(65)
1049	-	1055	δCH(72)
-	-	1045	νCCl(82), δ CH(14)
-	-	1033	γ CH(85)
1012	1011	1015	$\delta_{ipr}CH_3$(71)
-	-	1005	ρ_{rock} CH_2(69)
-	-	998	δ_{ring}(75)
-	-	996	δ_{ring}(75)
-	-	988	δ_{ring}(76)
-	-	981	δ_{ring}(75)

Cont..

Cont..

-	-	974	γ CH(68)
-	-	959	γ CH(68)
-	-	950	γ CH(68)
-	-	936	γ CH(67)
-	-	930	γ CH(68)
-	-	921	γ CH(68)
-	-	910	γ CH(68)
-	-	897	δ_{ipr} CH_3(71)
-	-	885	γ CH(67)
-	-	876	γ CCH_3(72)
-	-	871	δ_{ring}(75)
-	-	860	δ CCC(75)
853	852	852	γ CH(69)
-	-	843	γ CH(68)
-	-	837	σ_{sciss} NO_2(76)
-	-	832	γ CH(68)
817	-	820	γ CH(68)
-	-	807	γ CH(68)
-	-	799	γ CH(69)
781	-	784	γ CH(67)
-	-	771	γ CH(66)
-	-	754	γ CS(64), γ CN(17)
-	-	742	γ CH(59)
-	717	724	γ_{ring}(62)
711	-	714	γ_{ring}(62)
-	-	691	δ_{ring}(71)
-	-	674	γ_{ring}(63)
-	-	669	νCH(68)
-	-	650	δ_{ring}(65)
-	-	642	δ_{ring}(66)
-	631	634	γ CH(76)
-	-	619	γCS(65), δ CH(22)
595	-	597	γ_{ring}(69), γCH(13)
-	-	588	δ_{ring}(72)
-	-	582	δ_{ring}(75)
566	568	570	δ_{ring}(72)
-	-	553	γ CH(67)
-	-	544	δ CN(67)
-	-	523	γ CN (59)
-	-	511	γ CH(60)
-	-	499	γ CH(62)
485	482	486	$\rho_{rock}$$NO_2$ (73)
-	-	876	δ_{ring}(75)
-	-	465	γ_{ring}(70)
450	-	452	γ_{ring}(70)
-	-	444	γ CN (66)
-	-	436	γ_{ring}(58)
426	-	428	δ CC(62)
-	413	413	δ_{ring}(66)
-	-	406	γ_{ring}(63)
-	-	392	γ_{ring}(65)
-	362	364	γ_{ring}(58)
-	-	246	δ_{ring}(62)
-	-	329	γ CC(60)
-	-	305	δ CC(62)
-	-	291	δ CC(62)
-	-	278	γ CC(61)
-	258	257	δ CCl(63)
-	-	246	δ_{ring}(59)
-	-	228	δ_{ring}(58)
-	-	215	γ CN(57)
-	-	201	σ_{wagg} NO_2 (57)
-	-	188	τ CC(58)
-	-	164	τ CH_3(55)
-	-	155	τ CH_3(54)
-	-	147	γ CCl(58)
-	137	140	γ CC(60)
-	-	136	δ CC(63)
-	-	135	γ CC(56)
-	-	130	τ CC(60)
-	-	126	γ_{ring}(58)
-	-	118	γ_{ring}(58)
-	-	80	δ_{ring}(61)
-	-	73	δ CC(66)
-	-	68	δ CC(66)
-	-	64	τ NO_2 (58)
-	-	53	δ CC(61)
-	-	48	τ CC(54)
-	-	41	τ CC(58)
-	-	35	γ CC(56)
-	-	30	γ CC(54)
-	-	27	γ_{ring}(54)
-	-	21	γ_{ring}(54)
-	-	13	τ CC(52)
-	-	10	τ CC(50)

Cont..

ν - stretching, ν_{sym}- symmetric stretching, ν_{asym}- asymmetric stretching, δ - in-plane bending, γ - out-of-plane bending, scis - scissoring, w-wagging, rock-rocking,τ- torsion (out-of-plane bending)

eV, respectively. Hardness (η), softness (S), Electronegativity (χ) and electrophilicity index (ω) are usually called as global reactivity parameters. In this study, energy gap, electro negativity, electrophilicity index and hardness of the title

molecule were estimated B3LYP/cc-pVDZ method and the estimated values were listed in Table 3.

Reduced density gradient

The RDG analysis gets close to the real-space weak interaction, which is based on electron density and derivatives (Irfan et al.,2023). NCI-RDG analysis follows the graphic image of non-covalent interaction. It is a resolving and helpful technique, using a simple colour code to characterize steric interactions, van der Waals interactions and hydrogen bonds. RDG surface analysis enables investigation of interaction quality and strength. The blue color denotes strong hydrogen bond interaction; the red color represents strong repulsion and the green color implies van der Waals interaction (Fig.5.).

ELF & LOL analysis

ELF determines the localization of electrons in molecular systems (Jayaprakash et al., 2024). ELF is used to describe the aromaticity of a particle and the chemical bonding nature in transition metal centers. ELF value is close to one in the region of maximum Pauli repulsion and zero in the region of minimum Pauli repulsion. Fig. 6(a) graphically represents a 2-dimensional image of ELF. Fig. 6(b) shows its LOL distribution. The red color signifies a high ELF value, indicating the presence of 25 hydrogen atoms in the positive region for the title compound. Blue denotes the lowest ELF value. The least attractive atoms are O57, O58, N6, N7, N34, N56, and S33. A blue region surrounds these atoms. The LOL value is 0.98 au.

Molecular electrostatic potential surface

The purpose of this analysis is to investigate the electrophilic and nucleophilic boundary locationsthat influence the biological capacity of the molecule (Du et al., 2023). We visualize the molecule's relative polarity using the electrostatic potential surface. Fig.7. gives the MEP surface-

Table 3. Calculated frontier molecular orbital's energy values of CPDNT

Parameters	*B3LYP*
HOMO energy, E_{HOMO} (eV)	-5.555
LUMO energy, E_{LUMO} (eV)	-2.345
HOMO- LUMO energy gap, ΔE_{GAP} (eV)	3.211
Ionization potential, IP (eV)	5.555
Electron affinity, EA (eV)	2.345
Electronegativity, χ (eV)	3.950
Chemical hardness, η (eV)	1.605
Global softness, S $(eV)^{-1}$	0.311
Chemical potential, μ (eV)	-3.950
Electrophilicity index, ω (eV)	4.859
Total energy change, ΔE_T (eV)	-0.401
Overall energy balance, ΔE (eV)	-3.211

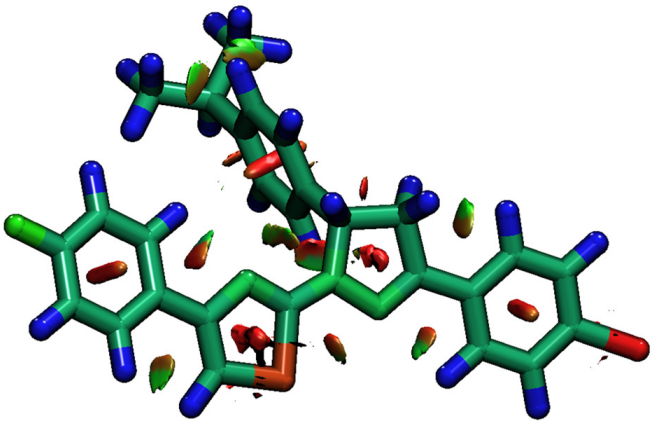

Figure 5. Iso density surface of RDG analysis

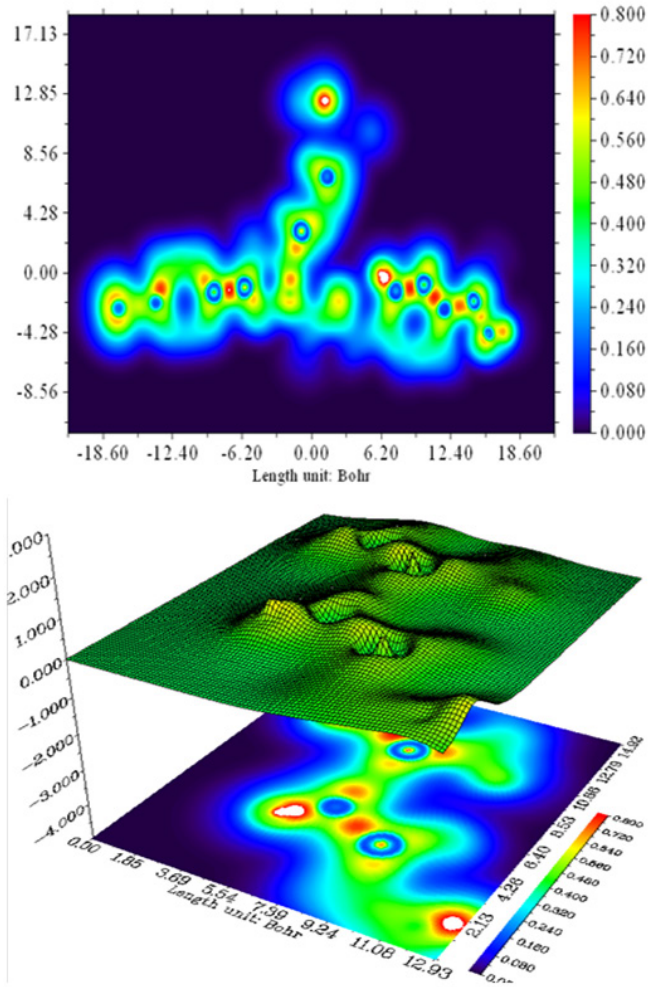

Figure 6: ELF and LOL surface maps of CPDNT compound

mapped isosurface range from -7.762e-2 to +7.762e-2. The O55 and O56 atoms of the nitro group primarily concentrate the most negative electrostatic potential, while the hydrogen-atom attached carbon atoms of the benzene ring display a red color. The blue color signifies the primary

Table 4: Molecular docking parameters of CPDNT ligand

PDB ID	Bond Length (Å)	Amino acid	Binding Energy (kcal/mol)	Inhibition constant (mM)	RMSD (Å)
1FSE	2.3	LYS A:30	-7.72	2.19	69.833
	2.1	LYS A:30			
3VZX	2.2	LYS A:17	-8.27	0.86	18.26
	2.2	LYS A:17			
5MKD	1.8	GLU A:36	-7.47	3.33	171.106
	1.8	ARG A:127			
LIXM	2.1	SER A:126	-8.39	0.71	81.956
	2.8	ASN A:131			

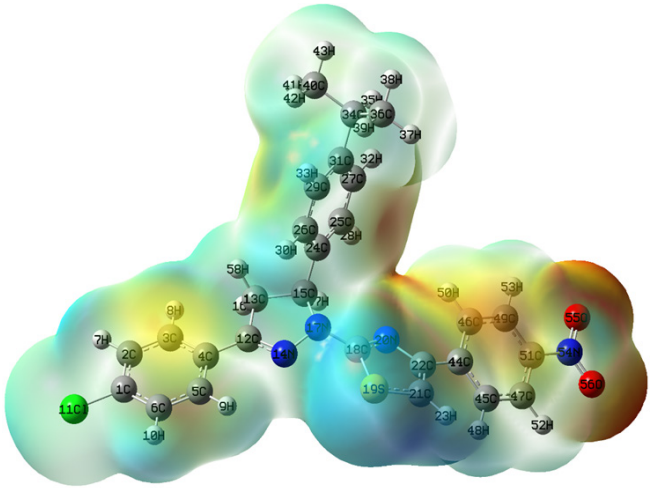

Figure 7: The surface mapping by electrostatic potential of CPDNT

concentration of positive electrostatic potential on the N54 atom of the nitro group, the S19 atom, and the hydrogen atoms.

Molecular docking

It is most frequently used to understand the protein-ligand interactions for the structure-based design of drugs (Miñarro - Lleonar et al., 2023). It involves placing a ligand molecule in the preferred site of binding of the target molecule, forming a complex, stable molecule. The structures of target proteins 1FSE, 3VZX, 5MKD, and 1IXM were attained from RCSB PDB format. Calculations were accomplished using Auto Dock-Vina software. Fig.8. displays the docking analysis of the CPDNT compound. Table 4 records the first three rank docking parameters for all four proteins.

These results indicate that CPDNT binds with 1FSE, 3VZX, 5MKD, and 1IXM with binding affinity of -7.72 kcal/mol, -8.27 kcal/mol, -7.47 kcal/mol, and -8.39 kcal/mol, respectively. The CPDNT ligand made two hydrogen bonds with the 1FSE protein's LYS30, one at 2.3 Å and the other at 2.1 Å. The binding result of 3VZX with CPDNT illustrates the binding site of LYS17, positioned at distances of 2.2 Å. GLU36 of the 5MKD protein contributes to the stabilization of the ligand

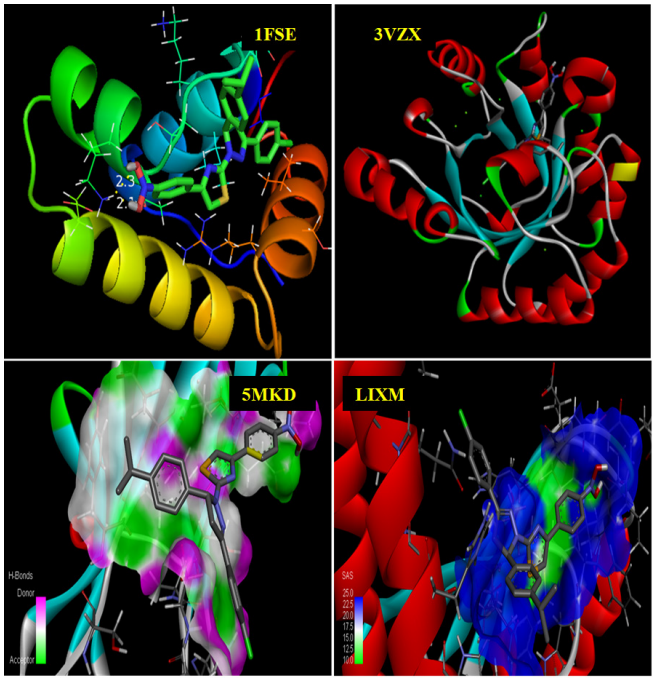

Figure 8: 3D images of interactions between ligand with target protein structures

CPDNT in the binding pocket, located at 1.8 Å. The CPDNT ligand formed three hydrogen bonds with the 1IXM protein's ARG127, SER126, and ASN131 with distances measured at 1.8, 2.1, and 2.8 Å, respectively. These molecules immobilized the CPDNT ligand within the binding pockets of the 1FSE, 3VZX, 5MKD, and 1IXM proteins.

Conclusion

The compound CPDNT was studied under vibrational spectroscopy, and its characteristics were determined. For the title compound, Optimized geometries, vibrational band intensityand vibrational wave number have been calculated using the B3LYP/cc-pVDZ, which shows good agreement with the outcomes that were observed. Spectroscopic analysis confirms the functional groups present in the CPDNT. The plot of calculated HOMO and LUMO has been given out for understanding the transfer of charge in the molecule.

The frontier molecular orbital calculations revealed a small value of the HOMO-LUMO energy gap of 3.211 eV, showing the chemically active. MEP analysis was accomplished, from which the nucleophilic and electrophilic regions were mapped. Molecular docking was accomplished for the CPDNT ligand with 1IXM protein, which displayed a large binding energy of -8.39 kcal/mol. Thus, the title compound formed a stable complex with this protein.

ACKNOWLEDGEMENTS

Nil.

References

Babiyana, S., Balachandran, V., Thirughanasambantham, N., Viji, A., Narayana, B., Salian, V. V., ... & Khaled, J. M. (2024). Spectroscopic characterizations, RDG and docking study of 2-[3-(4-chlorophenyl)-5-(4-(propane-2-yl) phenyl)-4, 5-dihydro-1H pyrozol-1-yl]-4-(4-fluorophenyl)-1, 3-thiazole. *Zeitschrift für Physikalische Chemie*, *238*(10), 1887-1914.https://doi.org/10.1515/zpch-2024-0598

Bachhar, V., Joshi, V., Shekher Mishra, S., Shukla, R. K., Bhargava, S., & Duseja, M. (2024). In-Vitro Antimicrobial, Antidiabetic and Anticancer Activities of Calyptocarpus Vialis Extract and Its Integration With Computational Studies. *ChemistrySelect*, *9*(35), e202401414.https://doi.org/10.1002/slct.202401414

Bhanwala, N., Gupta, V., Chandrakar, L., & Khatik, G. L. (2023). Thiazole heterocycle: an incredible and potential scaffold in drug discovery and development of antitubercular agents. *ChemistrySelect*, *8*(46), e202302803.https://doi.org/10.1002/slct.202302803

Bhasker, G., Salahuddin, Mazumder, A., Kumar, R., Kumar, G., Ahsan, M. J., ... & Kapoor, B. (2024). Hybrids of Benzimidazole-oxadiazole: A New Avenue for Synthesis, Pharmacological Activity and Recent Patents for the Development of More Effective Ligands. *Current Organic Synthesis*, *21*(8), 976-1013. https://doi.org/10.2174/0115701794260740231010111408

Cashman, J. R. (2020). Small Molecule Regulation of Stem Cells that Generate Bone, Chondrocyte, and Cardiac Cells. *Current Topics in Medicinal Chemistry*, *20*(26), 2344-2361.https://doi.org/10.2174/1568026620666200820143912

Chahal, M., Dhillon, S., Rani, P., Kumari, G., Aneja, D. K., & Kinger, M. (2023). Unravelling the synthetic and therapeutic aspects of five, six and fused heterocycles using Vilsmeier–Haackreagent. *RSC advances*, *13*(38),26604-26629.https://doi.org/10.1039/D3RA04309F

Dennington, R., Keith, T., & Millam, J. (2009). GaussView. Version 5, vol Shawnee Mission. Semichem.

Du, L., Geng, C., Zeng, Q., Huang, T., Tang, J., Chu, Y., & Zhao, K. (2023). Dockey: a modern integrated tool for large-scale molecular docking and virtual screening. *Briefings in Bioinformatics*, *24*(2), bbad047.https://doi.org/10.1093/bib/bbad047

Elangovan, N., Sowrirajan, S., Arumugam, N., Almansour, A. I., Altaf, M., Viswanathan, V., & Mahalingam, S. M. (2024). Computational investigation of molecular structure, spectral analysis, PES study and molecular docking studies of 4-(butan-2-ylideneamino) benzenesulfonamide. *Journal of Molecular Structure*, *1298*, 137054.https://doi.org/10.1016/j.molstruc.2023.137054

Frisch, M. J., Trucks, G. W., Schlegel, H. B., Scuseria, G. E., Robb, M. A., Cheeseman, J. R., Nakatsuji, H. (2009). Uranyl extraction by N, N-dialkylamide ligands studied by static and dynamic DFT simulations. *Gaussian*, *9*(9), 227.A.D. Becke, Real-space post-Hartree-Fock correlation models, J. Chem. Phys. 2005) 122, 064101. https://doi.org/10.1063/1.1844493

Ghomashi, R., Ghomashi, S., Aghaei, H., & Massah, A. R. (2023). Recent advances in biological active sulfonamide based hybrid compounds Part A: Two-component sulfonamide hybrids. *Current Medicinal Chemistry*, *30*(4), 407-480.https://doi.org/10.2174/0929867329666220722143547

Irfan, A., Hussien, M., Chaudhry, A. R., Qayyum, M. A., Al-Sehemi, A. G., Selvakumari, S., & Muthu, S. (2023). Effect of solvent role in electronic properties, band gap, electron injection barrier, charge transport nature, topology studies (ELF, LOL, RDG), and optical properties of azoles for multifunctional applications. *Journal of Molecular Liquids*, *390*, 122956.https://doi.org/10.1016/j.molliq.2023.122956

Jayaprakash, P., Selvaraj, S., & Kumar, A. R. (2024). A new organic compound (C9H12N2O2): crystal structure, characterization, Hirshfeld surface analysis, electronic properties, NLO properties, DFT calculation and molecular docking. *Solid State Sciences*, *154*, 107587.https://doi.org/10.1016/j.solidstatesciences.2024.107587

Kassem, A. F., Althomali, R. H., Anwar, M. M., & El-Sofany, W. I. (2024). Thiazole moiety: A promising scaffold for anticancer drug discovery. *Journal of Molecular Structure*, *1303*, 137510.https://doi.org/10.1016/j.molstruc.2024.137510

Liu, H., Xu, T., Xue, Z., Huang, M., Wang, T., Zhang, M., Guo, Y. (2024). Current development of thiazole-containing compounds as potential antibacterials against methicillin-resistant staphylococcus aureus. *ACS Infectious Diseases*, *10*(2),350-370. https://doi.org/10.1021/acsinfecdis.3c00647

Matta, R., Pochampally, J., Dhoddi, B. N., Bhookya, S., Bitla, S., & Akkiraju, A. G. (2023). Synthesis, antimicrobial and antioxidant activity of triazole, pyrazole containing thiazole derivatives and molecular docking studies on COVID-19. *BMCchemistry*, *17*(1), 61.https://doi.org/10.1186/s13065-023-00965-8

Miñarro-Lleonar, M., Bertran-Mostazo, A., Duro, J., Barril, X., & Juárez-Jiménez, J. (2023). Lenalidomide stabilizes protein–protein complexes by turning labile intermolecular H-bonds into robust interactions. *Journal of medicinal chemistry*, *66*(9), 6037-6046.https://doi.org/10.1021/acs.jmedchem.2c01692

Moeini, R., Memariani, Z., Asadi, F., Bozorgi, M., & Gorji, N. (2019). Pistacia genus as a potential source of neuroprotective natural products. *Planta medica*, *85*(17), 1326-1350.https://doi.org/10.1055/a-1014-1075

Neetha, S., Santhosh, C., Sheela, K., Ravi Singh, K., Sridhar, M., & Sadashiva, M. (2025). A comprehensive analysis of the molecular packing in the crystal of (4-methoxyphenyl) methyl 4-(4-chlorophenyl)-1, 3-thiazole-2-carboxylate: insights of X-ray crystallography and DFT analysis. *Journal of Molecular Structure*, *1319*, 139584.https://doi.org/10.1016/j.molstruc.2024.139584

Nemeikaitė-Čėnienė, A., Misevičienė, L., Marozienė, A., Jonušienė, V., & Čėnas, N. (2023). Enzymatic Redox Properties and cytotoxicity of irreversible nitroaromatic thioredoxin reductase inhibitors in mammalian cells. *International Journal of Molecular Sciences*, *24*(15), 12460.https://doi.org/10.3390/ijms241512460

Parr, R. G., & Yang, W. (1995). Density-functional theory of the electronic structure of molecules. *Annual review of physical chemistry*, *46*(1),701-728.https://doi.org/10.1146/annurev.pc.46.100195.003413

Patra, P., & Kar, G. K. (2021). The synthesis, biological evaluation and fluorescence study of chromeno [4, 3-b] pyridin/quinolin-one derivatives, the backbone of natural product polyneomarline C scaffolds: a brief review. *New Journal of Chemistry*, *45*(6), 2879-2934.https://doi.org/10.1039/D0NJ04761A

Ragavan, J. I., Anbarasan, P. M., Arunkumar, A., & Ibrahim, A. (2022). Design, Synthesis, Spectroscopic Characterization, Molecular Docking and Biological Evaluation of 9H-Carbazole Linked 4-Nitrophenol: A DFT Approach. *Journal of Computational Biophysics and Chemistry*, *21*(08), 909-926.https://doi.org/10.1142/S2737416522500259

Raveesha, R., Anusuya, A. M., Raghu, A. V., Kumar, K. Y., Kumar, M. D., Prasad, S. B., & Prashanth, M. K. (2022). Synthesis and characterization of novel thiazole derivatives as potential anticancer agents: Molecular docking and DFT studies. *Computational Toxicology*, *21*, 100202.https://doi.org/10.1016/j.comtox.2021.100202

Roy, T., Padhi, S., Mazumder, R., Majee, C., Das, S., Monika, Mishra & Kapoor, B. (2024). Alleviating neurodegenerative diseases associated with mitochondrial defects by therapeutic biomolecules. *Current Topics in MedicinalChemistry*, *24*(16),1377-1407.https://doi.org/10.2174/0115680266299148240329062647

Safaei, S., Mohammadpoor-Baltork, I., Khosropour, A. R., Moghadam, M., Tangestaninejad, S., & Mirkhani, V. (2012). Diastereoselective Synthesis of Pyrazolines using a Bifunctional Brønsted Acidic Ionic Liquid under Solvent-Free Conditions. *Advanced Synthesis&Catalysis*, *354*(16),3095-3104.https://doi.org/10.1002/adsc.201200191

Şahin, S. (2024). 2-(((2, 4-Dichlorophenyl) imino) methyl)-3, 4-difluorophenol: X-ray, DFT, MEP, HOMO-LUMO, NLO, Hirshfeld Surfaces, ADMET Profiling, Target Identification, Antipsychotic Activity Against Dopamine D2 and Serotonin 5-HT2A Receptors. *Gazi University Journal of Science*, *37*(1), 90-117.https://doi.org/10.35378/gujs.1241638

Saranya, P. V., Philip, R. M., & Anilkumar, G. (2024). Synthesis of imidazo [1, 2-a] pyridines via cobalt/iodine-catalyzed Ortoleva-King type approach. *Tetrahedron Letters*, *146*, 155188.https://doi.org/10.1016/j.tetlet.2024.155188

Sebutsoe, X. M., Tsotetsi, N. J. N., Jantjies, Z. E., Raphela-Choma, P. P., Choene, M. S., & Motadi, L. R. (2024). Therapeutic strategies in advanced cervical cancer detection,preventionandtreatment. *OncoTargets and Therapy*, 785-801.https://doi.org/10.2147/OTT.S475132

Shosha, M. I., El-Ablack, F. Z., & Saad, E. A. (2025). New thiazole derivative as a potential anticancer and topoisomerase II inhibitor. *ScientificReports*, *15*(1), 710.https://doi.org/10.1038/s41598-024-81294-1

Vidya, C., Jayaprakash, J., Ragavan, I., Shanavas, S., Priyadharsan, A., Acevedo, R., & Anbarasan, P. M. (2019). Synthesis, structural analysis, spectroscopic characterization and second order hyperpolarizability of 2-amino-4-methylpyridiniium-4-hydroxybenzolate crystal. *Journal of Materials Science: Materials in Electronics*, *30*(23), 20489-20505.

Viji, A., Balachandran, V., Babiyana, S., Narayana, B., & Salian, V. V. (2020). FT-IR and FT-Raman investigation, quantum chemical studies, molecular docking study and antimicrobial activity studies on novel bioactive drug of 1-(2, 4-Dichlorobenzyl)-3-[2-(3-(4-chlorophenyl)-5-(4-(propan-2-yl) phenyl-4, 5-dihydro-1H-pyrazol-1-yl]-4-oxo-4, 5-dihydro-1, 3-thiazol-5 (4H)-ylidence]-2, 3-dihydro-1H-indol-2-one. *Journal of Molecular Structure*, *1215*, 128244.https://doi.org/10.1016/j.molstruc.2020.128244

Zheng, H., Peng, X., Yang, S., Li, X., Huang, M., Wei, S., ... & Li, H. (2023). Targeting tumor-associated macrophages in hepatocellular carcinoma: biology, strategy, and immunotherapy. *Cell Death Discovery*, *9*(1), 65.https://doi.org/10.1038/s41420-023-01356-7